communications physics

Article

https://doi.org/10.1038/s42005-024-01762-y

Towards robust dichroism in angle-resolved photoemission

Check for updates

J. Schusser[1,2] ✉, H. Orio[1], M. Ünzelmann[1], J. Heßdörfer[1], M. P. T. Masilamani[1], F. Diekmann[3], K. Rossnagel[3,4] & F. Reinert[1]

Dichroic techniques are highly relevant in the field of topological materials, layered systems, and spin-polarized electronic states. Dichroism in angle-resolved photoemission is per se a matrix element effect, which depends on the initial and final states as well as on the perturbation by the light field. Although matrix element effects in ARPES such as dichroism are important for addressing properties of the initial state wave functions, the results can strongly depend on experimental geometry or final state effects. Combining experimental data on bulk WSe_2 taken at soft x-ray photon energies with state-of-the-art photoemission calculations, we demonstrate that a dichroic observable called time-reversal dichroism remains unaffected against variation of photon energy, light polarization, and the angle of incidence. We demonstrate a direct link of TRDAD obtained with both linearly and circularly polarized photons to the initial state properties indicating its broad applicability. The robustness of this matrix element effect indicates a considerable benefit over other dichroic techniques and encourages further experimental and theoretical investigations.

Angle-resolved photoemission spectroscopy (ARPES)[1,2] is arguably the most universal method to probe the electronic band structure of crystalline materials[3,4]. In the past decades there has been a lot of progress resulting in the development of ARPES-based modalities - soft X-ray, time-resolved[5], spin-resolved[6], and advanced combinations of these[7,8]. At the end of the last century, it was shown[2] that ARPES spectral weight depends on the transition dipole matrix element between the initial Bloch wave and the final states. However, for simplicity, it is often assumed that the photoemission intensity is proportional to a one-particle spectral function of the initial states, and matrix element effects are neglected, even though they have proven to be pivotal, for example, when identifying topologically non-trivial materials[9] or for disentangling the origin of "waterfall" dispersion in high-temperature superconductors[10]. Matrix-element effects and corresponding angular variation of ARPES spectral weight have been widely used to study the spin textures as well as the orbital textures[6,11–14]. Namely, linear (LD) and circular dichroism (CD)[15–19] in the angular distribution in ARPES have been useful in assessing (and under certain assumptions even proportional to) orbital angular momentum or Berry curvature[9,15,16] — quantities crucial for the classification of topological insulators or Dirac and Weyl semimetals. The continuous efforts in the field eventually led to finding observables such as time-reversal dichroism in photoelectron angular distributions (TRDAD)[20], intrinsic linear dichroism in photoelectron angular distributions (iLDAD)[21] or complex Fourier dichroism[22]. The discovery of a truly robust observable that provides direct access to the initial state properties would be of great importance. In this joint work, combining both photoemission experiment and state-of-the-art photoemission theory on the bulk transition metal dichalcogenide (TMDC) 2H-polytype WSe_2, we show that TRDAD proves to be a robust dichroic technique and remains stable under various changes in the matrix element. In particular, we discuss the robustness of TRDAD in the soft X-ray regime to determine whether the assumptions about its robustness will hold in a bulk-sensitive scenario. The TRDAD was tested in the context of experimental geometry, photon energy, and final state dependence. We not only prove the high robustness of the observable compared to other dichroic techniques but also show its versatility lingering in the fact that one can use both linearly and circularly polarized light sources and extract qualitatively very similar information. We (i) show that TRDAD methodology is much broader than previously predicted, (ii) show how TRDAD gives access to truly intrinsic initial state information and (iii) show a direct link of TRDAD to orbital angular momentum (OAM) and pseudospin. Considering the layered structure of WSe_2, in which adjacent trilayers are rotated by 180°, signal integration with increasing photon energy will eventually lead to averaging and consequent quenching of the dichroic signal. In addition, we discuss other effects such as phase dependence of the final state that comes into play at high photon energies. Hence, our work also touches on possible limitations of soft X-rays when used to

[1]Experimentelle Physik VII and Würzburg-Dresden Cluster of Excellence ct.qmat, Universität Würzburg, D-97074 Würzburg, Germany. [2]New Technologies-Research Center, University of West Bohemia, 30614 Pilsen, Czech Republic. [3]Ruprecht Haensel Laboratory, Deutsches Elektronen-Synchrotron DESY, D-22607 Hamburg, Germany. [4]Institute of Experimental and Applied Physics, Kiel University, D-24098 Kiel, Germany. ✉e-mail: schusser@ntc.zcu.cz

study materials with alternating layer structure where the wavefunction character of individual layers reverses.

Results

In any system with inequivalent K and K' valley introduced by inversion symmetry breaking, such inequivalence will be reflected in the corresponding pseudovector (orbital, spin, etc.) characterazing the initial state polarization. Such inequivalence can be accessed by TRDAD with sensitivity to the intrinsic component of such pseudovectors. To understand how TRDAD can be seen as an intrinsic version of linear dichroism (LD), the reader will easily agree that the intrinsic orbital texture of 2H-TMDC reflected in LD extracted under two distinct azimuthal orientations (0° and 60°), $I_{LD_{0°}}$ and $I_{LD_{60°}}$ spectra should be antisymmetric with respect to each other. The $I_{LD_{0°}}$ and $I_{\mathrm{LD}_{60°}}$ can, however, individually each contain certain extrinsic contribution which will be identical to the two spectra. An example of such an extrinsic contribution can be the contribution of trivial 3-fold symmetry or non-chiral contributions into the photocurrent. By subtracting the two during the extraction of TRDAD, these extrinsic contributions cancel, while the antisymmetric imprint of the orbital texture enhances. And while the TRDAD was originaly introduced with p-polarization, we will now show that an alternative using a c-polarized light gives qualitatively very similar information. To this end, we will introduce an alternative to standard TRDAD, namely circular-polarization generated TRDAD to which we will refer to as cTRDAD. The experimental geometry is shown in Fig. 1a, and the band dispersion measured as the sum of the spectra obtained with C_+ and C_- within the plane normal to the light incidence is shown in Fig. 1b. In Fig. 1c–j, we show the dichroic pattern in constant energy cuts (CEC) obtained from WSe_2 single crystals. Specifically, we consider the sum of measurements taken with left and right circularly polarized light incident on the sample along the Γ-M ($\beta = 0$) direction

$$I_\beta\left(k_x, k_y\right) = I_{\mathrm{C}_+}\left(k_x, k_y\right) + I_{\mathrm{C}_-}\left(k_x, k_y\right) \tag{1}$$

and extract the LD defined as

$$I_{\mathrm{LD}_\beta} = I_\beta\left(k_x, k_y\right) - I_\beta\left(-k_x, k_y\right). \tag{2}$$

This procedure has been done for data sets obtained under two distinct azimuthal sample orientations, i.e., $\beta = 0°$ and $\beta = 60°$. Rotating the sample by 60° is mathematically equivalent to imposing the time-reversal operation on the band structure $\mathcal{R}_{60°}\,|\psi^{\mathrm{K}}_{\mathbf{k}}\rangle \equiv \hat{T}|\psi^{\mathrm{K}}_{\mathbf{k}}\rangle = |\psi^{\mathrm{K}'}_{-\mathbf{k}}\rangle$. In Fig. 1, we now consider the difference of these signals:

$$\mathrm{cTRDAD} = \frac{I_{\mathrm{LD}_{60°}} - I_{\mathrm{LD}_{0°}}}{2}. \tag{3}$$

In analogy to the time-reversal dichroism (TRDAD) obtained with p-polarized light (which we will refer to as pTRDAD from now on)[20], we call the presented signal cTRDAD, specifying the use of summed circularly polarized light. We have subtracted the signal of two spectra obtained on WSe_2 samples rotated by 60° with respect to each other. To remain qualitatively as close as possible to the band dispersion, the difference of the two spectra was not divided by the sum of the two. Detailed extraction of theoretical (Supplementary Fig. 1) and experimental (Supplementary Figs. 2 and 4) cTRDAD can be found in the Supplementary Note 2.

To explain the qualitative similarity of c and pTRDAD we provide a detailed derivation of the corresponding matrix element mixing term for linear dichroism as defined by (2) in Supplementary Note 1 for $I_{\mathrm{LD}}^{\mathrm{C}_+ + \mathrm{C}_-}(k_x, k_y, k_z)$ and $I_{\mathrm{LD}}^{\mathrm{p}}(k_x, k_y, k_z)$. The expressions (5) and (7) in Supplementary Note 1 show a clear proportionality of the two LD to the $T_x^* T_z$ mixing term which implies sensitivity to the y-component of OAM L_y. As the link was already pointed out in the supplementary material of ref. 20 for pTRDAD, due to the extreme similarity of c/pTRDAD we can conclude that cTRDAD is also sensitive to orbital pseudospin defined as $\sigma_y^{K/K'}(\mathbf{k}) = \langle\psi^{K/K'}_{\mathbf{k}}|\hat{\sigma}_y|\psi^{K/K'}_{\mathbf{k}}\rangle$, where $\hat{\sigma}_y$ is the Y-Pauli operator. Additionaly, the formation of pseudospin arising from the coupling of wave functions $d_{\pm 2}$ and d_{z^2} is inherently conected to the formation of in-plane orbital angular momentum with alternating sign between the K and K' valleys. The comparison of the experimental and corresponding one-step model calculations in Fig. 1 shows that there is a high degree of experimental and theoretical cTRDAD agreement over a range of valence band binding energies. Despite the fact that (i) these data were extracted using C-polarized light and (ii) measured at significantly higher and thus more bulk-sensitive photon energies, the spectra show a reasonable agreement with those in ref. 20. This surprising observation indicates that TRDAD seems to be a robust quantity. In the following, we will thus analyze and discuss the dichroism under variation of certain experimental conditions.

We will first briefly examine the information depth of TRDAD. It was shown in ref. 20 that the TRDAD is sensitive to a pseudospin in the initial state wave function of WSe_2. The states at the valence band maxima at K/K' points can be written down in terms of a minimal model as $|\psi^{K/K'}_{\mathbf{k}}\rangle = C_{\pm 2}(\mathbf{k})|d_{\pm 2}\rangle + C_0(\mathbf{k})|d_{z^2}\rangle$[22]. This holds for a single layer WSe_2 in which inversion symmetry is broken and thus states of OAM $|d_{\pm 2}\rangle$ with an alternating sign between the K and K' valleys are formed. The particular

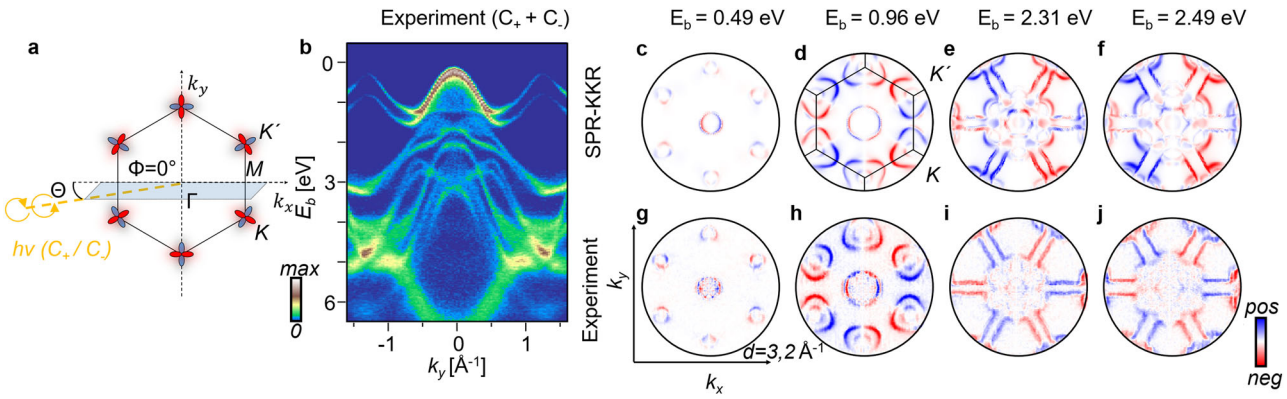

Fig. 1 | Experimental geometry, band dispersion and cTRAD CECs. The experimental geometry of the measurement is shown in **a**. θ defines the out-of-plane component of the incoming light, Φ changes the in-plane component. The band dispersion for the sum of circularly polarized light in **b** was extracted along the plane normal to the (blue) light incidence plane. Comparison of experimental and SPR-KKR c-TRDAD measured at $h\nu = 260$ eV with the sum of C_+ and C_- polarized lights at different binding energies. The photons arrive along Γ-X direction. **c–j** Comparison of one-step model to the experimental data. The cuts are extracted at **c**, **g** $E_b = 0.49$ eV, **d**, **h** $E_b = 0.96$ eV, **e**, **i** $E_b = 2.31$ eV, and **f**, **j** $E_b = 2.49$ eV, **d** contains a BZ scheme. The diameter of CECs d= 3,2 A.

pseudospin arises upon hybridization of those states with d_{z^2} orbitals giving rise to a likewise threefold symmetric TRDAD pattern, as observed in Fig. 1c–j.

In the case of inversion-symmetric bulk WSe_2, in turn, quenching of pseudospin – and consequently vanishing TRDAD pattern – would be expected. Contrary to this, we still see a TRDAD signal similar to a single monolayer. This types of 'hidden' spin[23,24], pseudospin[20], and orbital[25] polarization have been observed in spin-resolved and dichroic ARPES on layered bulk transition metal dichalcogenides and were explained with the high surface sensitivity of VUV-ARPES. In turn, this effect reduces upon increasing the photon energies and with that getting less sensitive to the uppermost layer. For instance, the measured photoemission spin polarization in bulk WSe_2 has been found to reduce to almost zero for $h\nu > 40$ eV[23]. In the present case, however, the observed cTRDAD is still noticeable for high photon energies of 260 eV, i.e., in the SX regime. We thus conclude that our TRDAD measurements in the soft X-ray regime still preserve sensitivity to pseudospin. At this point, it should also be noted, that we have conducted measurements at 460 eV, where the overall dichroism is strongly attenuated. In highly bulk sensitive (460 eV and 860 eV) regime where contributions of even and odd layers with opposite orbital character become comparable, an uniform sign reversal of TRDAD occurs. This can be explained by the phase of the final state which changes with increasing photon energy. The phase change consequently results in the amplitude of the final state oscillations to enhance the contributions from the lower laying layers. It is important to note that this (i) occurs only when the contribution of the even and odd layers are comparable and (ii) this only confirms the robustness of TRDAD as up to the sign, the qualitative information contained in TRDAD does not change. This is further supported by Supplementary Fig. 5.

We will now show how independent of geometry both pTRDAD and cTRDAD are. First, we measured in the same geometry with $\Phi = 0$ as shown in Fig. 1. Since conventional photoemission setups usually do not allow for a change in the direction of the incoming light, we used the relative rotation of the sample with respect to the analyzer and the light to mimic the situation in which the light arrives rotated by 90° to the earlier scenario. Further details of how this relative rotation is done are shown in Supplementary Fig. 3 in the Supplementary Note 2.

The corresponding experimental result is shown in Fig. 2a and demonstrates the independence of cTRDAD from experimental geometry. This is further illustrated by the one-step model in Fig. 2c–f, where by manipulating Φ, the in-plane component of the incident light is changed systematically, while the changes of the corresponding signal are negligible, according to the experimental observations. This implies robustness of TRDAD in general to the experimental geometry. Next, we discuss the qualitative difference between pTRDAD (as calculated in Fig. 2g–j) and cTRDAD (in Fig. 2c–f). An agreement between the two is immediately noticeable. More analysis is provided in Fig. 3 where cTRDAD and pTRDAD are compared. First, at 230 eV, the changes between the two become slightly more apparent - even though the two retain a high degree of correspondence in the first BZ, the further we move fromthe Γ point, the more weight will be gained by the "off-normal" component to the matrix element, and the signal of pTRDAD and cTRDAD does not necessarily maintain the one-to-one correspondence. Another effect to keep in mind is the acquired Bloch phase that comes into play and the corresponding slightly different effect on pTRDAD and cTRDAD.

Nonetheless, Fig. 3a, b prove that, even if the intensity of the corresponding CEC is not identical, the signal of the related TRDAD is very similar. This is also true for the four line profiles A–D in Fig. 3e extracted from four areas sketched in Fig. 3a. It is apparent that in these four areas, there are small, but finite differences between the two quantities as the photon energy changes. At the same time, it can be seen that the total sign of the signal remains the same.

Until now, in the SPR-KKR calculations, we have always used so-called time-reversal low energy electron diffracted (TR-LEED) final state to describe the photoelectron transition matrix element. Let us further discuss the importance of the final state in the matrix element. The p/cTRDAD in Fig. 3 and the corresponding line-profile extraction in areas A–D show that both magnitude and sign are robust against variation of hv once the TR-LEED final state is used. The impressive reliability of the TR-LEED final state is also discussed elsewhere[9,26,27]. For the purpose of this work, it is sufficient to note that unlike the free-electron (FE) final state, TR-LEED final state "feels" the environment of the solid — its analytical form depends on the scattering environment of each scattering site of the sample. This and the fact that its amplitude attenuates in the crystal are the main features that cannot possibly be captured by the FE final state description of the three-step model. From previous work[9], it immediately follows that the final state description itself is defining for the correct representation of LD and CD. Figure 3 shows, however, that it is also critical for the TRDAD, and once the simplified FE approximation is used in Fig. 3c, d, the overall observables discussed here are no longer captured properly. Despite the fact that Fig. 3e shows somewhat similar behavior for both TRDAD with FE final state, their corresponding sign is not preserved over the range of photon energies used here. This implies that all of these observables are sensitive to the environment of the sample. This inherently local property of TRDAD may further contribute to the discussion of whether dichroism, in general, is sensitive to local "atomic" orbital angular momentum or to non-local orbital angular momentum manifolds, as understood by the "modern theory of polarization"[9,15]. The $h\nu$ evolution of the signal with the TR-LEED final state is much less pronounced and can most likely be attributed to simple k_z-dispersion evolution.

To unambiguously determine to which intrinsic hidden initial state property the cTRDAD is sensitive to, one needs to consider the underlying symmetry of the measured sample. As seen from the Supplementary Fig. 6 and the explanation there, we can confidently claim that TRDAD in 2H-WSe_2 is sensitive to hidden inversion symmetry breaking (ISB) stemming from the W atoms. From the discussion present there it becomes apparent that in 1T polytypes (with inversion symmetric trilayers) one becomes sensitive to the "intrinsic" OAM within the topmost layer due to different photoelectron yield from different chalcogenide atoms. Accessing hidden properties is nicely demonstrated in ref. 28, where analog to TRDAD (in a system with different symmetry) is used to remove the "spurious" trivial contributions of the crystal to extract so-called "intrinsic chiral circular dichroism" (icCD) which by subtracting two LD spectra in different crystal orientations removes contributions coming from the simple 4-foldness of the system and is sensitive to electronic chirality.

Finally, we point out a few experiment-relevant aspects. One reason for using $C_+ + C_-$ is the proof of principle and the limitation of the experimental setup used. As the matrix element terms of p-polarized and summed circularly polarized lights are to a high degree similar, our work also provides a pathway to obtaining more direct information about quantities such as initial state orbital symmetries (usually addressed with linearly polarized light) with circularly polarized photons where the capabilities of different experimental facilities need to be considered. Additionaly, our approach allows for accessing L_y component of OAM which is conventionally not accessible in measurements with circularly polarized light (with light incidence along x-z plane). While the x- and z- components are conventionally accessed by CD measurements, using the sum of the two circular polarizations gives access to a linearly independent third component of OAM allowing for a complete methodology.

Due to the two WSe_2 terminations present at different domains (and their 180° rotated orientation with respect to each other) on one sample and the three-fold symmetry of the $P6_3/mmc$ (194) space group, it would have been possible to perform the experiment without actually having to rotate the sample. The two domains represent the two sample orientations necessary for the TRDAD extraction, further facilitating the experimental use of the relevant observables. When scanning for the rotated domain, one needs to make sure of the dominant single-domain contribution. Experimental observation that moving from one to the other domain gives qualitative identity to the results obtained with rotating by 60° confirms that the TRDAD in the adjacent trilayers reverses sign. Besides the sign reversal, its distribution over the BZ remains the same.

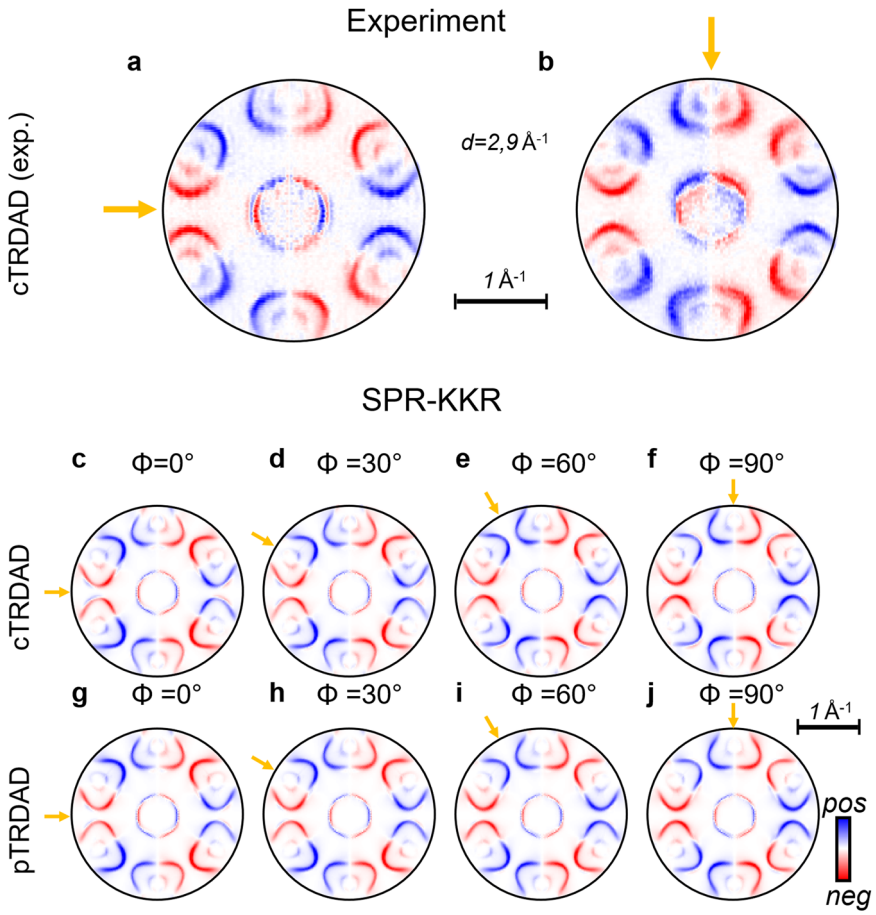

Fig. 2 | Systematic change of the in-plane component of the incoming light for CEC at $E_b = 0.96$ eV. a and **b** show experimentally measured time-reversal dichroism in photoelectron angular distributions with c-polarized light (cTRDAD) corresponding to geometries with light (orange arrow) arriving from the left in **a** and from the top in **b**. The spectra were measured at $h\nu =$ 260 eV. Qualitative comparison of pTRDAD and cTRDAD and their dependence on experimental geometry as delivered by the spin-polarized relativistic Korringa–Kohn–Rostoker (SPR-KKR). **c**–**f** show the systematic change of the in-plane component of the incoming light by rotating it from 0° to 90° for cTRDAD. **g**–**j** show the same for time-reversal dichroism in photoelectron angular distributions obtained with p-polarized light (pTRDAD). The red and blue in the color bar indicate positive and negative values, respectively. The scale bars are 1 Å.

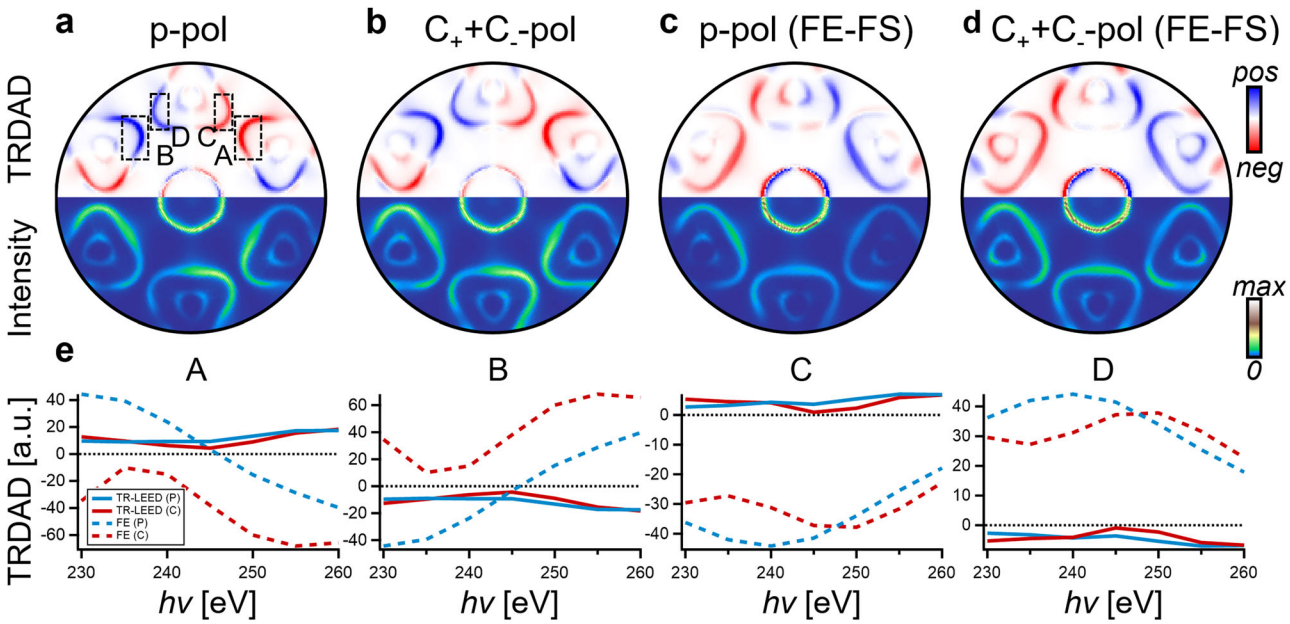

Fig. 3 | One-step model intensity and corresponding time-reversal dichroism in photoelectron angular distributions (TRDAD) with time-reversed low-energy electron diffraction (TR-LEED) and free-electron (FE) final states for constant energy cuts (CEC) at $E_b = 0.96$ eV. a Intensity and pTRDAD (TRDAD obtained with p-polarized light), **b** intensity and cTRDAD (TRDAD obtained with c-polarized light), both with TR-LEED final state. **c** and **d** contain respectively the same information, yet with FE final state. Cuts **a**–**d** were extracted for $h\nu = 230$ eV. **e** Shows corresponding signal changes in TRDAD with photon energy in areas A–D as sketched in **a**. Full red (blue) lines in **e** represent TR-LEED extracted with c- (p-) polarized light. Dashed lines correspond to FE final states with the same color coding for the polarization.

Another methodological point to make is that, unlike in refs. 20,21 where a time-of-flight detector (TOF) was used, we have acquired the experimental spectra using a hemispherical analyzer with deflectors. Such a setup, unlike those where one needs to rotate the sample to obtain full BZ information, preserves the matrix element of the photoemission process in the same fashion as in TOF measurements.

Conclusions

In conclusion, this study has provided a significant advance towards a complete methodology to map the energy- and momentum-dependent complex wave functions. In particular, this work has presented both experimental and theoretical observations that prove the extreme robustness of TRDAD and extend its potential use to the soft x-ray photon energies. To do this, we have shown analytical equivalence of LD generated with linearly polarized and a sum of circularly polarized lights to introduce cTRDAD. This allowed us to directly link cTRDAD to OAM and pseudospin. We have shown the qualitative similarity of cTRDAD to pTRDAD that can be used in experimental setups with sole access to circularly polarized light. With its almost independence from experimental geometry or photon energy, TRDAD in general as a robust photoemission tool provides much more direct access to the wave-function properties of the initial state. Due to certain qualitative similarities of LD and CD[14,15], we also expect that another modification of TRDAD which uses a difference of circularly-polarized light should in principle carry similar information to c/pTRDAD and gives access to orbital pseudospin. Our findings which are further discussed in the Supplementary Notes 1–3 will be relevant to other materials — not only to TMDCs within the trigonal prismatic phase (2H), but also to other three-fold and four-fold symmetric systems. Given the alternating trilayer structure of WSe_2 and the bulk-sensitive photon energies used, this study will also contribute to the debate of hidden photoemission observables such as hidden spin polarization or dichroism buried in alternating structures[29,30].

Methods

Experimental details

The experimental part of this work was performed at the soft x-ray beamline P04 of PETRA III at DESY with higly (>90%) circularly polarized synchrotron light and $h\nu = 260–460$ eV. The incident photons arrived at the sample along the *xz*-plane under the angle of incidence $\theta = 17°$ with respect to the sample surface. The Scienta DA30 analyzer slit is oriented in the plane parallel to the incoming light. The energy and angular resolutions were better than 90 meV and 0.1°. During the experiment, the pressure was better than 3×10^{-10} mbar, and the sample temperature was kept below 50 K.

Theoretical details

The theory was supplemented by the state-of-the-art one-step model based Spin-polarized-relativistic Korringa–Kohn–Rostoker (SPR-KKR) package which has proven to be highly reliable in reproducing photoemission data, details of which are discussed elsewhere[31]. The package takes into account sample termination and accurately represents all the photoelectron transition matrix-related phenomena, resulting in highly accurate photoemission spectra simulations. The versatility of SPR-KKR in modeling physical systems has been demonstrated not only on TMDCs[22,32,33], but also on simple systems such as Pd[34], heterostructures[35] or topologically non-trivial systems such as TaAs[34]. By nature of the multiple scattering formalism, a highly accurate multiply-scattered time-reversed low energy electron diffraction (TR-LEED)[26,27] is the default final state choice. Nonetheless, the final state can be tinkered with, higher scattering terms can be neglected, and the state can be reformulated into simplified expressions such as single-site scattered or free-electron-like. We have used the structurally identical model of WSe_2 as in ref. 20. Due to the different inelastic mean-free path of the photoelectrons, however, the imaginary part of the final state was changed to match the experimental data also in the 200–300 eV regime ($V_{0i} = 1.0$ eV). The inelastic mean free path (IMFP) is treated by intoduction of the finite imaginary part V_{0f} of the effective potential for the final state, the penetration depth of photons is considered to be much higher than the IMFP.

Data availability

The data that support the findings of this study are available from the corresponding author upon reasonable request.

Received: 15 December 2023; Accepted: 31 July 2024;
Published online: 08 August 2024

References

1. Reinert, F. & Hüfner, S. Photoemission spectroscopy - From early days to recent applications. *N. J. Phys.* **7**, 97 (2005).
2. Hüfner, S. et al. Photoemission spectroscopy in metals: Band structure-fermi surface-spectral function. *J. Electron Spectrosc. Relat. Phenom.* **100**, 191–213 (1999).
3. Damascelli, A. Probing the electronic structure of complex systems by ARPES. *Phys. Scr. T* **T109**, 61–74 (2004).
4. Moser, S. An experimentalist's guide to the matrix element in angle resolved photoemission. *J. Electron Spectrosc. Relat. Phenom.* **214**, 29–52 (2017).
5. Dakovski, G. L., Li, Y., Durakiewicz, T. & Rodriguez, G. Tunable ultrafast extreme ultraviolet source for time- and angle-resolved photoemission spectroscopy. *Rev. Sci. Instrum.* **81**, 073108 (2010).
6. Bentmann, H. et al. Strong Linear Dichroism in Spin-Polarized Photoemission from Spin-Orbit-Coupled Surface States. *Phys. Rev. Lett.* **119**, 1–6 (2017).
7. Bühlmann, K. et al. Compact setup for spin-, time-, and angle-resolved photoemission spectroscopy. *Rev. Sci. Instrum.* **91**, https://doi.org/10.1063/5.0004861 (2020).
8. Fanciulli, M. et al. Spin, time, and angle resolved photoemission spectroscopy on WTe2. *Phys. Rev. Res.* **2**, 1–5 (2020).
9. Schusser, J. et al. Assessing Nontrivial Topology in Weyl Semimetals by Dichroic Photoemission. *Phys. Rev. Lett.* **129**, 246404 (2022).
10. Liu, Y. et al. Anomalous high-energy waterfall-like electronic structure in 5 d transition metal oxide Sr2 IrO4with a strong spin-orbit coupling. *Sci. Rep.* **5**, 1–8 (2015).
11. Bawden, L. et al. Hierarchical spin-orbital polarization of a giant Rashba system. *Sci. Adv.* **1**, e1500495 (2015).
12. Cao, Y. et al. Mapping the orbital wavefunction of the surface states in three-dimensional topological insulators. *Nat. Phys.* **9**, 499–504 (2013).
13. Zeljkovic, I. et al. Mapping the unconventional orbital texture in topological crystalline insulators. *Nat. Phys.* **10**, 572–577 (2014).
14. Ünzelmann, M. et al. Orbital-Driven Rashba Effect in a Binary Honeycomb Monolayer AgTe. *Phys. Rev. Lett.* **124**, 176401 (2020).
15. Ünzelmann, M. et al. Momentum-space signatures of Berry flux monopoles in the Weyl semimetal TaAs. *Nat. Commun.* **12**, 3650 (2021).
16. Schüler, M. et al. Local Berry curvature signatures in dichroic angle-resolved photoelectron spectroscopy from two-dimensional materials. *Sci. Adv.* **6**, eaay2730 (2020).
17. Cho, S. et al. Studying local Berry curvature in 2H-WSe2 by circular dichroism photoemission utilizing crystal mirror plane. *Sci. Rep.* **11**, 1684 (2021).
18. Hagiwara, K. et al. Link between Weyl-fermion chirality and spin texture. http://arxiv.org/abs/2205.15252 (2022).
19. Min, C. H. et al. Orbital Fingerprint of Topological Fermi Arcs in the Weyl Semimetal TaP. *Phys. Rev. Lett.* **122**, 116402 (2019).
20. Beaulieu, S. et al. Revealing Hidden Orbital Pseudospin Texture with Time-Reversal Dichroism in Photoelectron Angular Distributions. *Phys. Rev. Lett.* **125**, 216404 (2020).
21. Beaulieu, S. et al. Unveiling the orbital texture of 1T-TiTe2 using intrinsic linear dichroism in multidimensional photoemission spectroscopy. *npj Quantum Mater.* **6**, 93 (2021).

22. Schüler, M. et al. Polarization-Modulated Angle-Resolved Photoemission Spectroscopy: Toward Circular Dichroism without Circular Photons and Bloch Wave-function Reconstruction. *Phys. Rev. X* **12**, 1–8 (2022).
23. Riley, J. M. et al. Direct observation of spin-polarized bulk bands in an inversion-symmetric semiconductor. *Nat. Phys.* **10**, 835–839 (2014).
24. Cheng, C., Sun, J. T., Chen, X. R. & Meng, S. Hidden spin polarization in the 1T-phase layered transition-metal dichalcogenides MX2 (M = Zr, Hf; X = S, Se, Te). *Sci. Bull.* **63**, 85–91 (2018).
25. Cho, S. et al. Experimental Observation of Hidden Berry Curvature in Inversion-Symmetric Bulk 2H-WSe2. *Phys. Rev. Lett.* **121**, 186401 (2018).
26. Braun, J., Minár, J., Ebert, H., Katsnelson, M. I. & Lichtenstein, A. I. Spectral function of ferromagnetic 3d metals: A self-consistent LSDA +DMFT approach combined with the one-step model of photoemission. *Phys. Rev. Lett.* **97**, 227601 (2006).
27. Berglund, C. N. & Spicer, W. E. Photoemission studies of copper and silver: Theory. *Phys. Rev.* **136**, A1030–A1044 (1964).
28. Brinkman, S. S. et al. Chirality-Driven Orbital Angular Momentum and Circular Dichroism in CoSi. *Phys. Rev. Lett.* **132**, http://arxiv.org/abs/2404.02952 (2024).
29. Clark, O. J., Dowinton, O., Bahramy, M. S. & Sánchez-Barriga, J. Hidden spin-orbital texture at the Γ-located valence band maximum of a transition metal dichalcogenide semiconductor. *Nat. Commun.* **13**, 4147 (2022).
30. Zhang, X., Liu, Q., Luo, J. W., Freeman, A. J. & Zunger, A. Hidden spin polarization in inversion-symmetric bulk crystals. *Nat. Phys.* **10**, 387–393 (2014).
31. Ebert, H., Ködderitzsch, D. & Minár, J. Calculating condensed matter properties using the KKR-Green's function method - Recent developments and applications. *Rep. Prog. Phys.* **74**, 096501 (2011).
32. Heider, T. et al. Geometry-Induced Spin Filtering in Photoemission Maps from WTe2 Surface States. *Phys. Rev. Lett.* **130**, 146401 (2023).
33. Ono, R. et al. Surface band characters of the Weyl semimetal candidate material MoTe2 revealed by one-step angle-resolved photoemission theory. *Phys. Rev. B* **103**, 125139 (2021).
34. Tan, X. L. et al. Soft X-ray Fermi surface tomography of palladium and rhodium via momentum microscopy. *Ultramicroscopy* **253**, 113820 (2023).
35. Geldiyev, B. et al. Strongly anisotropic spin and orbital Rashba effect at a tellurium - noble metal interface. *Phys. Rev. B* **108**, 1–7 (2023).

Acknowledgements

We would also like to thank J. Buck, M. Kalläne, and M. Hoesch for their support during the synchrotron measurements at PETRA III. This work was funded by the Würzburg-Dresden Cluster of Excellence on Complexity and Topology in Quantum Matter – *ct.qmat* (EXC 2147, project-id 390858490) and by the DFG through SFB1170 "Tocotronics" and directly via RE 1469/13-2. We acknowledge DESY (Hamburg, Germany), a member of the Helmholtz Association HGF, for the provision of experimental facilities. Parts of this research were carried out at PETRA III. Funding for the photoemission spectroscopy instrument at beamline P04 (Contracts 05KS7FK2, 05K10FK1, 05K12FK1, and 05K13FK1 with Kiel University; 05KS7WW1 and 05K10WW2 with Würzburg University) by the Federal Ministry of Education and Research (BMBF) is gratefully acknowledged. We also thank Ján Minár for allowing J.S. to use the computation cluster at the New Technologies Research Centre at the University of West Bohemia. We have used the Munich SPR-KKR package, version 7.7, H. Ebert et al., http://ebert.cup.uni-muenchen.de/SPRKKR.

Author contributions

J.S., H.O., J.H. and M.P.T.M. performed the experiments, J.S. performed the photoemission calculations and analyzed the experimental and theoretical data. F.D. and K.R. provided the WSe_2 samples. All authors contributed to the discussion of the manuscript. J.S. wrote the manuscript with contributions from M.Ü. and F.R. J.S. conceived and planned the project.

Funding

Open Access funding enabled and organized by Projekt DEAL.

Competing interests

The authors declare no competing interests.

Additional information

Supplementary information The online version contains supplementary material available at https://doi.org/10.1038/s42005-024-01762-y.

Correspondence and requests for materials should be addressed to J. Schusser.

Peer review information *Communications Physics* thanks the anonymous reviewers for their contribution to the peer review of this work.